THE UNUSUAL QUASAR PG1407+265

Jonathan C. McDowell[1], Claude Canizares[3], Martin Elvis[1], Andrew Lawrence[2], Sera Markoff[3,4], Smita Mathur[1], Belinda J. Wilkes[1]

Astrophysical Journal, 1995 Sep 10, in press

ABSTRACT

PG1407+265, discovered in the Palomar-Green Survey (Schmidt and Green 1983), was identified as a redshift one radio-quiet quasar on the basis of a single weak line. Further observations over a wide wavelength range confirm the identification, but reveal the object to have unusual emission line properties. Broad Hα is the only strong emission line, with Hβ and Lyman α almost undetectably weak. The emission lines show a range in redshift of over 10000 km/s, systematically decreasing with ionization potential, or almost equivalently, increasing to longer wavelengths. $z = 0.94 \pm 0.02$ is a reasonable statement of our knowledge of the quasar's redshift. However, the object's continuum properties are those of a normal radio-quiet quasar. We discuss a number of possible models for the object, but its nature remains puzzling.

Subject headings: Galaxies: Quasars

[1]Center for Astrophysics, 60 Garden Street, Cambridge, MA 02138

[2]University of Edinburgh

[3]Massachussets Institute of Technology, Cambridge MA

[4]Dept. of Physics and Steward Observatory, University of Arizona

1. Introduction

In the course of our survey of quasar continuum energy distributions (Elvis et al 1994), we realized that the redshift of one of our sample objects, PG1407+265, was not secure. The assignment of $z = 0.944$ by Schmidt and Green (1983) was based on a single extremely weak line identified as Mg II λ2798. Noisy IUE spectra obtained in 1983 and 1987 did not reveal any further lines. Confidence in the identification was increased with the publication of a high quality optical spectrum by Schneider, Schmitt and Gunn (1991) which showed weak FeII emission in addition to the Mg II line, but a 1989 IUE spectrum of improved quality by P. O'Brien failed to show any evidence for hydrogen Lyman α.

We have carried out a comprehensive multiwaveband study (Table 1) of this object as part of our larger survey of quasar properties (Elvis et al 1994). Our optical spectrophotometry showed no evidence for significant variability over a baseline of ten years; this and the radio-quiet nature of the source make it unlikely that it is related to BL Lac objects. The X-ray flux detected by the Einstein and ROSAT satellites is at the level expected for a quasar, and the continuum shape is normal with an ultraviolet bump of median strength and, as expected, an inflection at between 1 and 2 microns in the putative rest frame. Nevertheless, the equivalent width of Lyman α ($\sim 8\mathring{A}$) is extremely low compared to other objects (20-80$\mathring{A}$, Francis et al 1991).

2. Observations

2.1. Optical Spectrophotometry

We obtained optical spectrophotometry of the quasar during 1988 at the Multiple Mirror Telescope (MMT) using the Blue Channel and the Faint Object Grating Spectrograph (FOGS). Higher resolution data were obtained through a one arcsecond slit and the flux level was normalized using lower resolution data through a five arcsecond slit. Mg II and CIII emission lines are detected, together with strong FeII emission. In an attempt to observe the region around rest frame Hβ, I.W. Browne, P.N. Wilkinson and D. Henstock kindly obtained Faint Object Spectrograph (FOS) data on the 2.5m Isaac Newton Telescope (INT) extending to 10000A. Unfortunately the spectral region in question sits on atmospheric absorption lines, but the presence of an Hβ line of normal strength can be ruled out. The normalization of all the spectra is in good agreement with CCD photometry obtained at the 0.6m telescope of the F.L. Whipple Observatory in 1986. The combined optical spectrum is presented in Fig. 1.

2.2. Ultraviolet Observations

The IUE spectra were retrieved from the National Space Science Data Center and analysed using the RDAF IDL package. The spectra were extracted and calibrated using the standard GEX Gaussian Extraction algorithm (Urry and Reichert 1988). HST data, taken as part of the Absorption Line Key Project (Bahcall et al 1993) were retrieved from the Hubble Data Archive using Starview and analysed with the STSDAS package. We adjusted the flux of the G160L observation, taken through the 0.1 arcsecond aperture, to match the data in the other gratings, taken through the 0.25 x 2.0 arcsecond slit. We note that the G270H spectrum was not analysed by Bahcall et al. since it covers wavelengths longwards of Lyman α. Weak OIV+SiIV and CIV lines are present in the HST spectrum (Fig. 2), and (less obviously) in the IUE data. The Lyman-α line is present, but cut up with superimposed absorption lines. Our value of 8Å for the equivalent width of this line is approximate and based on an ad hoc linear continuum fit at 1300A and 1140A. (Table 2). The HST data agree well in flux (to within 15 percent) with the 1989 and 1986 IUE data; the quasar's far ultraviolet flux seems to have increased by 30 percent since the 1983 IUE observation. This degree of variability is normal in quasars (Kinney et al 1991).

2.3. Infrared Observations

IR spectroscopy was obtained through a service observation carried out on UKIRT (the United Kingdom Infrared Telescope). The spectrum shown in Fig. 3, which shows a strong Hα line at an observed wavelength of 1.28 microns, was obtained on 1994 Jan 29 with the cooled grating spectrometer CGS4, using the 150 mm camera, and a 75 lines/mm grating in second order, resulting in a spectral resolution corresponding to 780 km/sec. One resolution element is approxmately equal to one detector pixel; however the detector was stepped in increments of 1/3 of a pixel to improve sampling. The slit width used was 3", roughly equal to one original detector pixel. Standard nodding, calibration, and atmospheric correction techniques were followed. Because of the large slit size, the wavelength calibration could potentially be offset if the object was not properly centred; any such error is certainly less than 400 km/sec, and probably much less.

JHKL photometry was obtained at the MMT in 1988, and shows the continuum inflection characteristic of a quasar. Examination of the IRAS sky images shows that PG1407+265 is 3 arcmin from the strong 60 micron source IRAS14070+2636, which has been identified with the starburst galaxy Haro 40. Addscans of the IRAS survey data show no evidence for a 60 micron detection of the quasar, but we have reported a formal, marginal 25 micron detection (Elvis et al 1994) although this should probably be treated with scepticism as it was not detected in any other IRAS band.

2.4. X-ray Observations

PG1407+265 was observed on 1992 Jan 19 with the ROSAT PSPC (Trümper 1983, Pfeffermann et al 1987) for 3229 sec. The source is well detected, and is consistent with the point spread function. We note that there is no evidence for any significant confusing source at the position of Haro 40 (Green et al 1989), with a 3 sigma upper limit of 1×10^{-13} erg cm^{-2} s^{-1} (0.4-2.4 keV).

We extracted counts from a 3 arcminute circle around the position of PG1407+265, together with background in an annulus from 3.5 to 7 arcminutes, using the IRAF/PROS package. The data were analysed with the XSPEC spectral fitting package using the Jan 1993 (DRM 36) response matrix. We fit a single power law spectrum with Galactic absorption (Morrison and McCammon 1983). The data are consistent with this model and the fitted absorption was consistent with the Galactic value of $1.38{\pm}0.10 \times 10^{20}$ cm^{-2} (Elvis, Lockman and Wilkes 1989), so we repeated the fit with absorption fixed at this value. The best fit gave a power law energy index of 1.61 ± 0.05 and a 1 keV flux of $1.0 \pm 0.04\mu$Jy, with a reduced χ^2 of 0.49 (Fig. 4). Consistent results were obtained using the SPECTRAL package in IRAF/PROS. We also set an upper limit to the amount of extra absorption (above Galactic) due to cold material at the redshift of the source of $N_H < 3.1 \times 10^{20}$cm^{-2} (or $4.9{\times}10^{19}$cm^{-2} for extra absorbers at zero redshift); although there are no obvious edges in the spectrum, we cannot rule out the presence of an ionized absorber. Our derived power law index is steeper than, but consistent with, the Einstein IPC result of $1.2^{+0.9}_{-0.2}$ (Wilkes and Elvis 1987); note that fits to PSPC data appear systematically steeper than the IPC (Fiore et al 1994). The normalization, however, is more than twice as high as the IPC value of 0.44 μJy, indicating significant X-ray variability over a timescale of a decade.

3. Results

3.1. The Redshift of PG1407+265

The initial published redshift estimate (Schmidt and Green 1983) was based on the single MgII line. The failure to detect other lines in our intermediate signal-to-noise spectrophotometry and in the IUE data raised the possiblity that alternate (even non-quasar) identifications might be possible (Elvis et al 1994).

Our observation of the strong Hα line in the near infrared and our identification of the weak CIV and OIV]+SiIV lines in the HST data provide conclusive evidence that the redshift of the object is indeed near unity. The high quality spectrum of Steidel and Sargent (1991) claimed to confirm the redshift as z=0.947, and identified emission redward of MgII as due to the λ2950 FeII feature. However the feature they claimed as CIII] (observed wavelength 4019.4A, their table 1) is inconsistent with this redshift; the feature corresponds to a weak unidentified line in the composite spectrum of Francis et al (1991), and is not as strong in our MMT data. The true CIII]+Al III feature is the weaker one visible in their spectrum at approximately the correct rest wavelength.

The wavelengths of the peaks of each emission line were measured and used to derive redshift estimates (Table 2). We quote nominal '1 sigma' uncertainties which are one third of our eyeball estimates of the maximum uncertainty in the peak location. As is typical for quasars, the redshifts of the low ionization lines are larger than those of the high ionization lines (Gaskell 1982, Wilkes 1984, Espey et al 1989). However the range in redshift for PG1407+265 is an order of magnitude larger than typically seen; 10200 ± 1200 km s^{-1} between Hα and CIV compared with $\sim$1000 km s^{-1} in the earlier studies. The wavelength scales of the various instruments should be much better than this; the optical spectra were taken with the slit vertical to avoid refraction effects, while this is not an issue for the ultraviolet spectra, and refraction is small enough in the infrared to compensate for the larger slit width. Uncertanties in the velocity scale due to slit width and refraction effects should be less than 500 km/s in all cases.

Figure 5 shows the various emission lines on a common velocity scale with zero point set by Mg II. We see a significant trend of the velocity shift to increase with the ionization potential of the emission line (Fig 6a). We note that a trend with rest wavelength is almost equivalent (Fig 6b). We suggest that $z=0.94\pm0.02$ is a reasonable statement of our knowledge of the quasar's redshift. Note in Figure 5 that there is a narrow absorption feature in Lyman α coincident with the velocity of the Hα emission line, implying some overlaid neutral hydrogen component.

We also measured approximate line widths and fluxes. CIV λ1549 and the broad component of Hα both have full width half max (FWHM) around 7000 km/s. MgII has a similar component but with a broad red-wing 'shelf' of blended FeII UV multiplets leading to a formal FWHM of around 12000 km/s. CIII] λ1909 appears to be equal in flux with Al III λ1858, although our spectrum has low signal-to-noise in this region.

3.2. Line properties

The emission lines in PG1407+265 appear unusually weak by eye. How extreme are these equivalent widths? Table 2 gives the details of our measured values, including estimates of the integrated rest frame luminosity in each line. Typical emission line properties of quasars are given in Table 12.4 of Osterbrock (1989), and for a subset of lines in Francis et al (1991). While the Osterbrock data is not based on any specific sample, the latter paper gives average properties of the well-defined Large Bright Quasar Survey. Further, Francis (1993) gives histograms of equivalent width for the bright ultraviolet lines which may be used to measure how unusual PG1407+265 actually is, although their spectral signal to noise is too low to give reliable measurements for individual objects at the low equivalent widths we are probing.

The OIV] equivalent width, W(OIV]), is relatively normal in PG1407+265, only a factor of two low. However W(Lα) is in the bottom three percent of the Francis et al distribution (typical values 30-100$\AA$), as is the CIV strength (typically 20-50$\AA$), while W(MgII) is in the lowest 4 percent of its corresponding distribution (typical values 50-80$\AA$). Quasar Hα equivalent widths are still hard to find, with results from several groups (Baker et al 1994, Baker 1994) indicating that typical values are in the range 250-1200$\AA$, consistent with the early data of Baldwin (1975). However we note that three objects in the sample of Espey et al (1989) have values between 140 and 150 $\AA$, comparable to our value of W(Hα)=126$\AA$. We may summarize by saying that most of the line *ratios* in PG1407+265 are not exceptional within the large uncertainties, but the equivalent widths for the principal lines are anomalously weak by factors of 3 to 10. In contrast, the FeII multiplets (both optical and UV) appear to be unusually strong.

3.3. Continuum properties

In contrast to the lines, the continuum properties of PG1407+265 are remarkably normal. We present the dereddened, rest frame infrared to X-ray energy distribution in Fig. 7, and a close-up of the optical to ultraviolet region in Fig. 8. The radio-loudness (log of 5 GHz to optical B band flux) is 0.28, within the normal range (Kellerman et al 1989, Elvis et al 1994) for radio-quiet objects. The 8 mJy, 5 GHz radio source is unresolved, although there is a probably unrelated weak source one arcminute away (Kellerman et al 1994). The blue bump strength is log (L(1000-2000$\AA$)/L(0.8-1.6μm)) = 0.69, indistinguishable from the median value of 0.66 for the UVSX sample of Elvis et al (1994), of which it is a member (see Fig.6, which shows the 68 percentile ranges of that sample). The absolute continuum level in our 1988 MMT observations agrees with the Neugebauer et al (1987) Palomar observations made in 1980 to within 15 percent, as seen in a number of other objects in the Elvis et al survey. IUE and HST observations are consistent with mild variations typical of quasars (Kinney et al 1991). The presence of an inflection in the energy distribution between H and K, the Einstein IPC X-ray spectral index of 1.2 and ROSAT index of 1.6, and the low radio flux (Kellerman et al 1989), are all consistent with a normal, non-variable, radio-quiet quasar. The factor 2 variability in the X-ray flux is somewhat unusual but not unprecendented for high luminosity quasars (Zamorani et al 1984). There is therefore no evidence for any underlying variable, beamed, blazar-like continuum component which may reduce the strength of the emission lines in some flat-spectrum radio quasars.

4. Discussion

The emission line spectrum of PG1407+265 is unlike that of any other radio-quiet quasar we have seen, e.g. out of $\sim$ 100 in Elvis et al (1994), Kinney et al (1991), Boroson and Green (1993). In Fig. 8, we contrast the 1000-8000Å rest frame spectrum of PG1407+265 with comparable data for the ordinary, low redshift quasar PG1211+143. The difference in the amount of energy in the ultraviolet lines is dramatic. We now consider several possible explanations for the weak lines and differential redshifts of PG1407+265.

1. *Not a quasar*: Prior to the detection of Hα, we had speculated that the object might not be a quasar at all. That line and the overall multiwavelength continuum properties rule out that possibility.

2. *A beamed continuum*: The lines are washed out by a beamed, non-thermal component (a jet along the line of sight). This solution, which would be unprecedented in a radio-quiet object, is ruled out by the lack of continuum variability, and the normal shape of the energy distribution.

3. *Low BELR covering factor:* The broad emission line region has a lower covering factor, intercepting less of the continuum radiation. This simple explanation accounts for the low equivalent widths of the emission lines which originally drew our attention to the object, but does not address the bizarre CIV and OIV line shifts.

4. *Abnormal photoionizing continuum:* The weakness of the lines is intrinsic and due to an abnormal photoionizing continuum as seen by the line emitting region. Although the continuum we see is normal, we may be looking at a special angle. If there is obscuration between the central source and most of the BELR (except along our line of sight) this might occur, although we have not tried to reproduce the observed spectrum with a photoionization code. Since objects like PG1407+265 are clearly rare (a few percent at most), explanations involving special geometry are reasonable.

5. *Time lags:* The UV continuum has recently brightened and the lines have not yet caught up. The lack of optical and UV variability on a ten year timescale casts doubt on this, although the factor two increase in the X-ray since 1981 is worth noting. This explanation would imply an effective BELR radius large compared with ten light years, while scaling with the expected $L^{1/2}$ dependence from NGC5548 (Clavel et al 1991) would predict a much smaller BELR radius, $\sim$ 1 light year.

6. *Abnormal BELR physical properties:* The weakness of the lines is intrinsic and due to abnormal cloud properties in the broad emission line region. Before the detection of Hα the possibility of 'hydrogen depleted' clouds was tenable (if physically unlikely). The presence of Hα requires some other peculiarity: the size or density of the clouds

may be unusual, or the distance of the BELR gas from the central object may be abnormal, leading to an unusual ionization parameter.

7. *FeII dominated continuum:* the emission lines have a normal equivalent width with respect to the true continuum but are masked by strong FeII emission as in IRAS07598+6508 (Lawrence et al 1988). This might work for some of the optical lines but cannot contribute to the weakness of CIV and Lyman α.

8. *Dust absorption:* The weakness of the short wavelength lines is due to patchy reddening between us and the quasar nucleus. This is unlikely since the continuum source shows no evidence of reddening: the ultraviolet continuum is strong and the soft X-rays show no significant absorption in excess of Galactic. The absence of a definite IRAS detection implies (Fig. 6) that the object is not exceptionally far infrared bright, unlike some of the Fe II emitters studied by Lawrence et al (1988), and so most of the continuum cannot be reprocessed by dust. Any explanation based on reddening must therefore explain how the lines but not the continuum are affected.

9. *Line absorption:* PG1407+265 is a weak BAL quasar in which the absorption lines are eating away at the emission. Note that the Lyman α region (Fig 3) appears to contain narrow absorption lines, although there is no evidence for any Lyman continuum break so $N_H \leq 10^{17}$ cm^{-2}. Patchy absorption leaves the continuum source unaffected while most of the BELR emission is soaked up in a BAL region lying between us and the high ionization region of the BELR generating CIV and OIV]. This explanation can address the observed redshift differences. The velocity of the BAL clouds is such that the red wing and center of the BELR lines are preferentially absorbed. The remaining blue wing gives an artificially low redshift. The low ionization emission lines, which are generated further from the nucleus, suffer less or no red BAL absorption and give the true emission redshift, which is nearer to z=0.95. The problem with this picture, as with dust absorption, is the low probability that the bulk of the emission lines would be absorbed without affecting the continuum source.

10. Gravitational amplification: The equivalent widths are low because the continuum source is magnified by a stellar mass microlens along the line of sight. Dalcanton et al (1994) set probabilities on the cosmological density of lensing objects based on the absence of weak equivalent width objects in some quasar samples; to cast their argument slightly differently, if microlensing has any significant effect on the quasar population, we should expect it to show up in a few high luminosity, bright objects with weak equivalent widths. PG1407+265 is a factor 25 more luminous than the median PG quasar from Schmidt and Green (1983), and only a magnitude less luminous that the multiple-image lens PG1115+080. This interpretation would predict that the continuum is likely to fade on a timescale of decades (for a 1

solar mass lens, Dalcanton et al 1994). However, the apparent strength of the FeII emission, which would be unlensed, counts against this explanation. A quantitative measurement of the strength of FeII(opt), not really possible with our current data due to the low signal to noise near Hβ, would be important in evaluating the possibility of lensing. Deep CCD imaging could reveal the presence of any lensing galaxy at $z \sim 0.5$.

5. Conclusion

We have presented observations of an unusual quasar, PG1407+265. The quasar has a normal non-variable, radio-quiet continuum energy distribution but the high ionization emission lines are extremely weak and strongly blueshifted with respect to the low ionization lines. We have discussed nine possible explanations for the unusual spectrum, none of which is immediately convincing. Higher signal-to-noise observations of the lines and detailed modelling will be required to resolve the mystery of PG1407+265.

We acknowledge support from STScI grant AR-3686.01-91A, NASA grants NAGW5-2201 (LTSA), NAS5-30934 (RSDC), and use of IPAC's National Extragalactic Database (NED), the Goddard Space Flight Center's IUE data analysis facility and HEASARC X-ray archive, and of the Hubble Data Archive.

REFERENCES

Bahcall, J., et al, 1993, ApJS 87, 1.

Baldwin, J., 1975, ApJ 201, 26.

Baker, A.C., et al, 1994, MNRAS 270, 575.

Baker, J.C., 1994, Ph.D. Thesis, University of Sydney.

Boroson, T., and Green, R.F., 1993. ApJS 80, 109.

Clavel, J., et al, 1991, ApJ 366, 64.

Dalcanton, J.J., Canizares, C.R., Granados, A., Steidel, C.C., and Stocke, J.T., 1994, ApJ 424, 550.

Elvis, M., et al, 1994 ApJ 95, 1.

Elvis, M, Lockman, F.J., and Wilkes, B.J., 1989. AJ 97, 777.

Espey, B., et al, 1989, ApJ 342, 666.

Fiore, F., et al, 1994 ApJ 431, 575.

Francis, P. J., et al, 1991. ApJ 373, 465.

Francis, P. J, 1993. ApJ 405, 119.

Gaskell, C.M., 1982, ApJ 263, 79.

Green, P.J., Ward, M.J., Anderson, S.F., Margon B., De Grijp M., and

Miley, G.K., 1989. ApJ 339, 93.

Kellerman, K.I., et al., 1989. AJ 98, 1195.

Kellerman, K.I., et al., 1994. AJ 108, 1163.

Kinney, A., et al., 1991. ApJS 75, 645.

Lawrence, A., et al, 1988, MNRAS 235, 261.

Morrison, R. and McCammon, D.A., 1983 ApJ 270, 119.

Osterbrock, D., 1989. Astrophysics of Gaseous Nebulae and Active Galactic Nuclei (Univ. Sci. Books: Mill Valley, CA).

Pfefferman, E., et al, Proc SPIE, 733, 519.

Schmidt M., and Green, R.F, 1983. ApJ 269, 352.

Steidel, C.C., and Sargent, W.L.W., 1991. ApJ 382, 433.

Trumper 1983, Adv. Space Res. 2, No. 4, 241.

Wilkes, B.J., 1984, MNRAS 207, 73.

Wilkes, B.J., and Elvis, M., 1987. ApJ 323, 343

Table 1: Log of Observations

Telescope[1]	Instrument[1]	Date	Exp (min)	Spectral range	Observers	ID [2]
Einstein	IPC	1981 Jan 17	26	0.2-3.5 keV	CfA	I05381
IRAS	Survey	1983		12-100μm	[Survey]	
VLA		1983 Nov		5 GHz	Kellerman et al	
FLWO 0.6m	CCD	1986 May 14		BVRI	Wilkes	
MMT	IR Photom.	1988 Apr 7		JHKL	Willner	
MMT	FOGS	1988 Apr 9		4500-8300$\AA$	Wilkes	
MMT	Blue Channel	1988 Jun 6		3200-6200$\AA$	Wilkes	
IUE	SWP	1983 Apr	356	1250-2000$\AA$	Snijders	SWP19858
IUE	LWP	1986 Dec	400	2000-3100$\AA$	Bechtold	LWP09733
IUE	LWP	1989 May 28	412	2000-3100$\AA$	O'Brien	LWP15616
IUE	SWP	1989 May 28	395	1250-2000$\AA$	O'Brien	SWP36351
ROSAT	PSPC	1992 Jan 19	54	0.15-2 keV	Canizares	RP700359
HST	FOS/H19	1992 Mar 9	18	1590-2300$\AA$	Bahcall et al	Y0RV0C03T,04T
HST	FOS/H27	1992 Mar 9	18	2200-3250$\AA$	Bahcall et al	Y0RV0C05T
HST	FOS/L15	1992 Mar 9	11	1170-2500$\AA$	Bahcall et al	Y0RV0C06T
UKIRT	CGS4	1994 Jan 29	8	1.15-1.36μm	UKIRT Service	
INT	FOS	1994 Feb 12	10	3650-10000$\AA$	Browne, Wilkinson, Henstock	

1. See main text for explanation of abbreviations.2. Sequence number or other designation in archive.

Table 2: PG1407+265: Measured Rest Frame Emission Line Properties

Line	Instrument	λ_{obs}	Redshift	EW ($\AA$)	Luminosity (10^{44} erg s^{-1})	Typical EW[1] ($\AA$)
Lyα λ1215	IUE	-	-	< 10	30–100	
	HST	2370	0.95±0.015	8±3	10:	
OIV]+SiIV λ1400	IUE	2690	0.92±0.01	9.1 ± 3	4.2	
	HST	2675	0.912±0.004	4.3 ±2	2.2	
CIV λ1549	IUE	2960	0.91±0.01	3.6±2.5	1.5	20–50
	HST	2980	0.924±0.004	4.6±2	1.9	
CIII]+Al III $\lambda\lambda$1909,1858	MMT/Blue	3700	0.94±0.03	9.9	3.5	
MgII λ2798	MMT/Blue	5435	0.943±0.003	23.5	4.6	50-80
	MMT/FOGS	5450	0.948±0.0012	23.2	4.8	
	INT	5445	0.946±0.002	11.6	2.2	
	SS91[2]		0.947	24.4		
Hβ λ4861	INT		-	<40	<2.2	
Hα λ6563	UKIRT	12850	0.958±0.001	126.0	4.1	250-1200

1) Typical equivalent widths for the samples of Francis (1993), Espey et al (1989), Baker et al (1994), Baker (1994).
2) Steidel and Sargent (1991).

Urry, C.M., and Reichert, G., 1988, NASA IUE Newsletter 34, 95.

Zamorani, G et al, 1984. ApJ 278, 28.

This preprint was prepared with the AAS LaTeX macros v3.0.

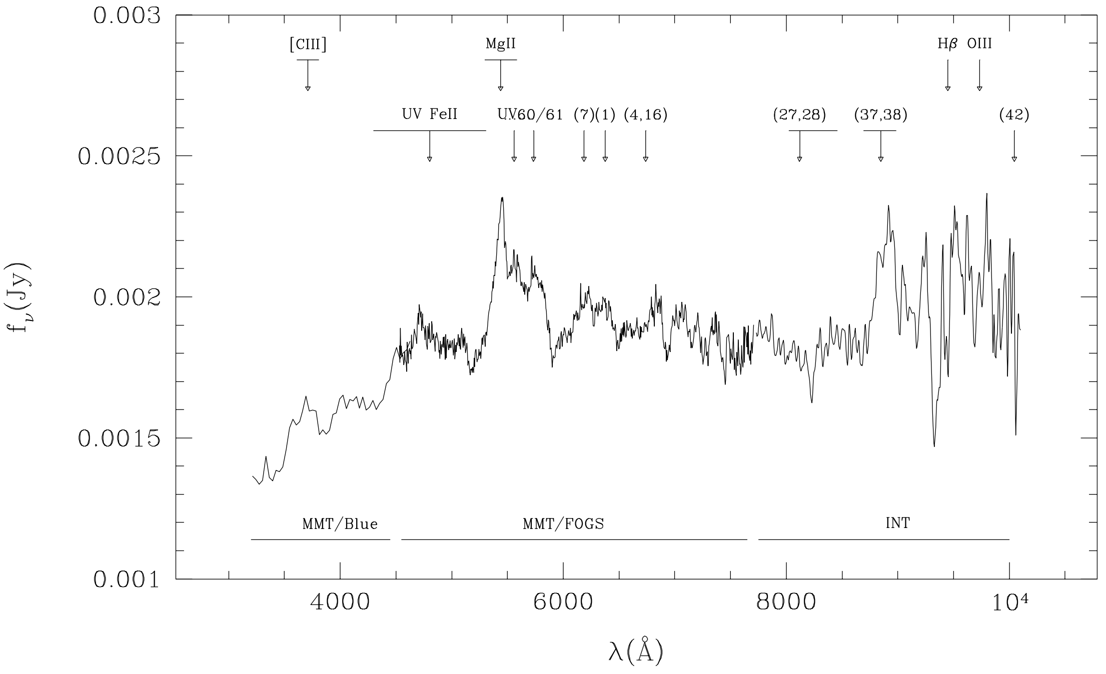

Fig. 1.— Optical spectrum of PG1407+265. The plot shows the combined observations from the MMT Blue channel and FOGS instruments and the INT. Expected locations of emission lines and selected Fe II multiplets are indicated. The Blue channel and INT data have been multiplied by a constant 12 percent factor to agree with the FOGS data.

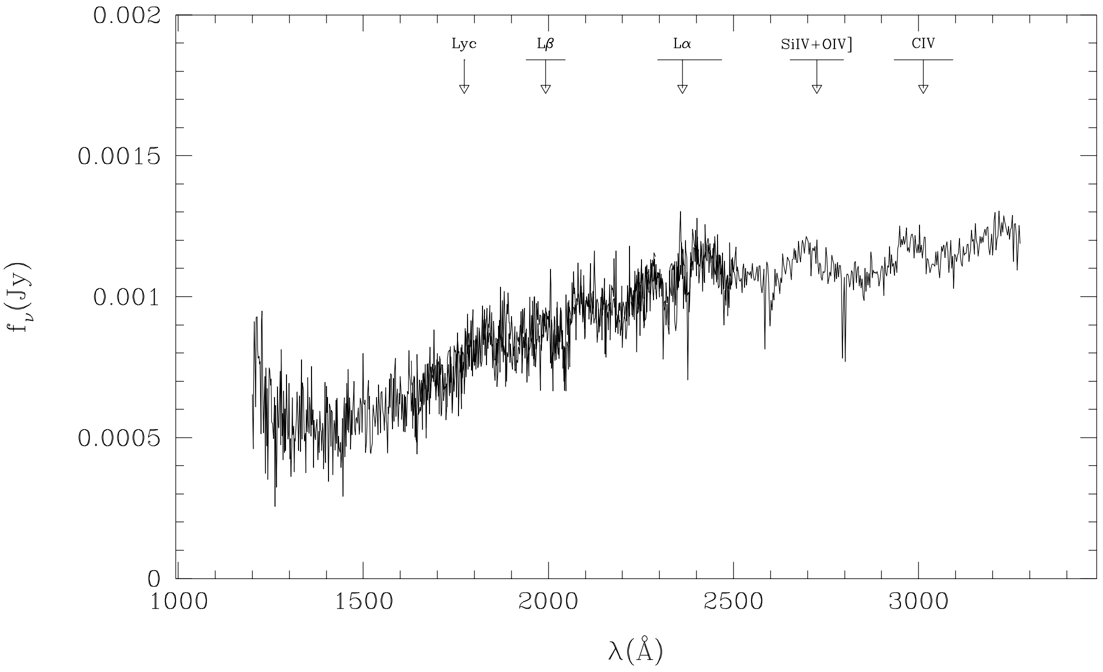

Fig. 2.— HST spectrum of PG1407+265. The plot shows the combined observations from the G270H, G190H and G160L gratings.

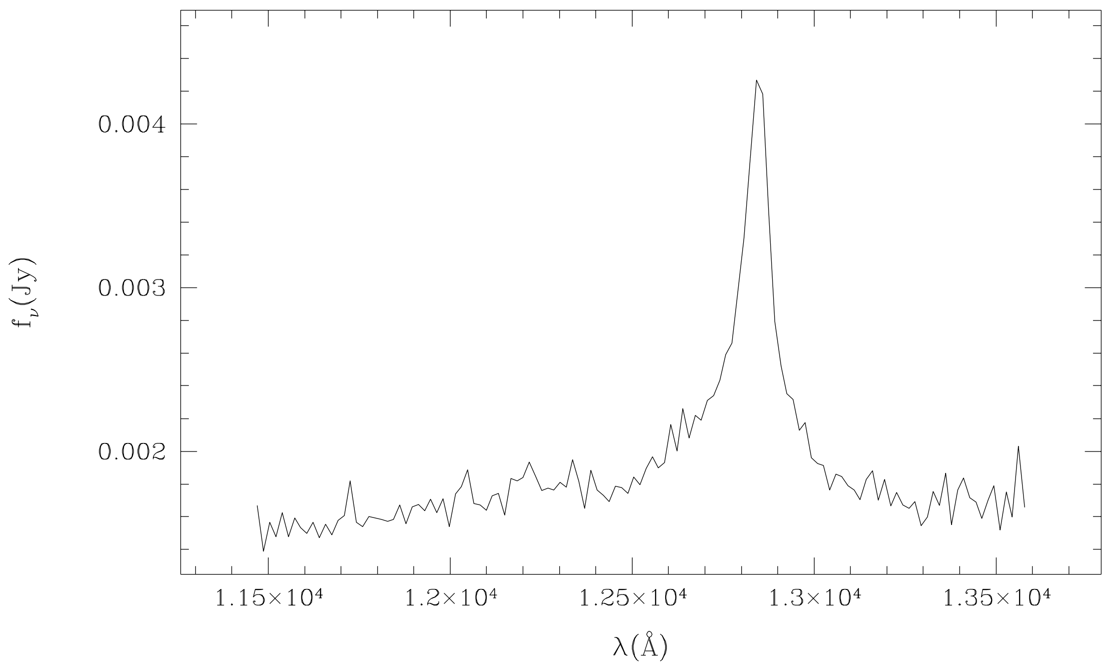

Fig. 3.— Infrared spectrum of PG1407+265, obtained as a UKIRT service observation on 1994 Jan 29.

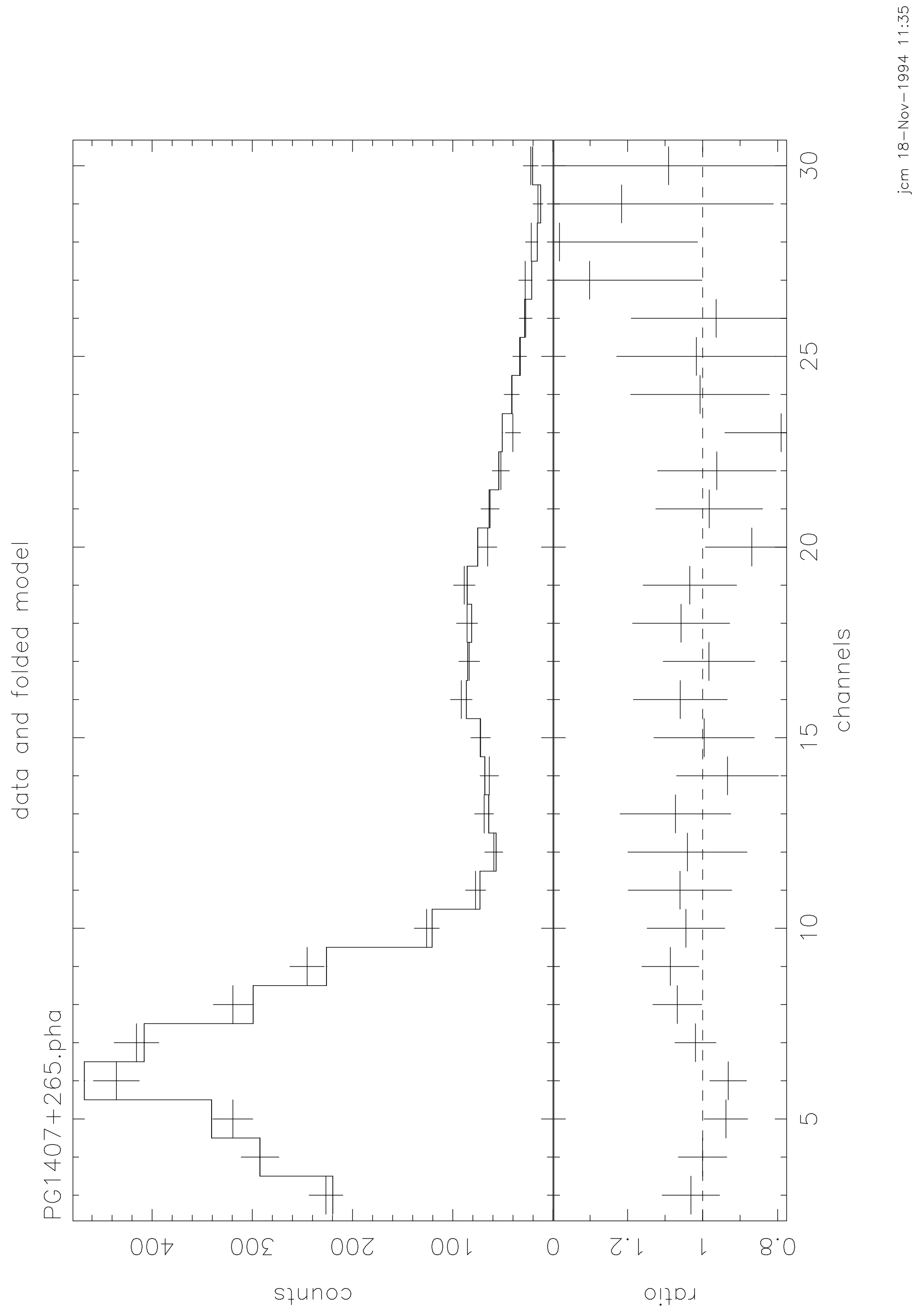

Fig. 4.— ROSAT PSPC pulse height spectrum of PG1407+265. The upper panel shows the extracted counts (crosses) and the fitted power law model (solid line) while the lower panel shows the ratio of the counts to the model in each channel. The power law model includes Galactic absorption of 1.38×10^{20} cm^{-2}.

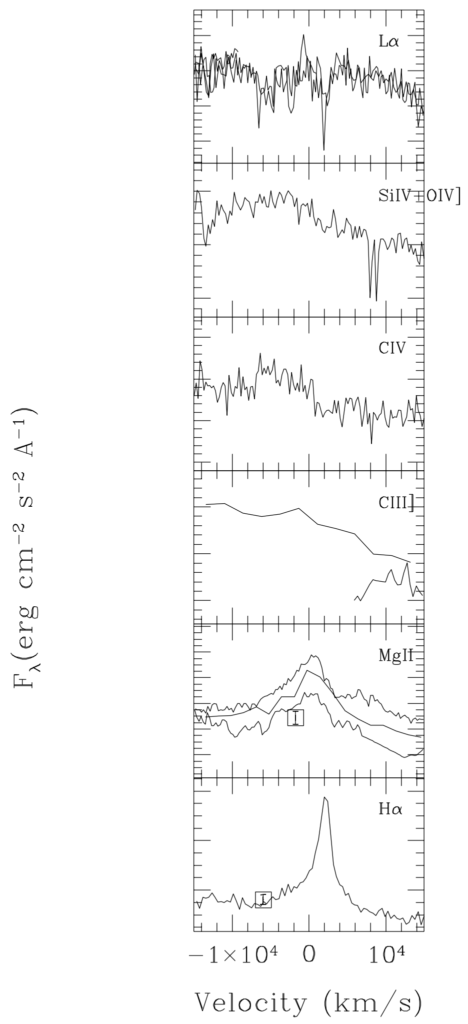

Fig. 5.— PG1407+265 emission lines plotted on a common velocity scale. The zero point corresponds to the Mg II redshift. There are several Mg II spectra superposed (MMT Blue, FOGS, and the INT data), and two HST exposures superposed for Lyman α. Squares in Mg II and Hα boxes correspond to broad band photometry measurements.

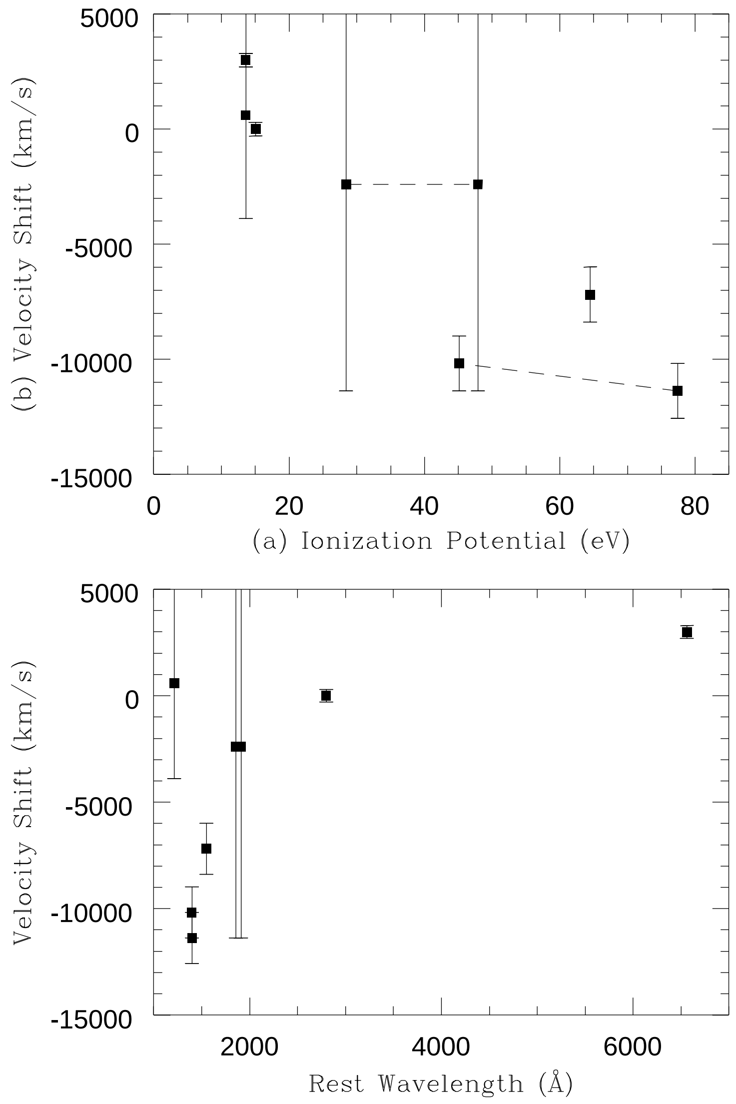

Fig. 6.— PG1407+265 estimated line velocities versus (a) ionization potential, (b) rest wavelength. The velocity zero point corresponds to the Mg II redshift. The dashed lines in (a) connect the components of line blends, since those points are not independent.

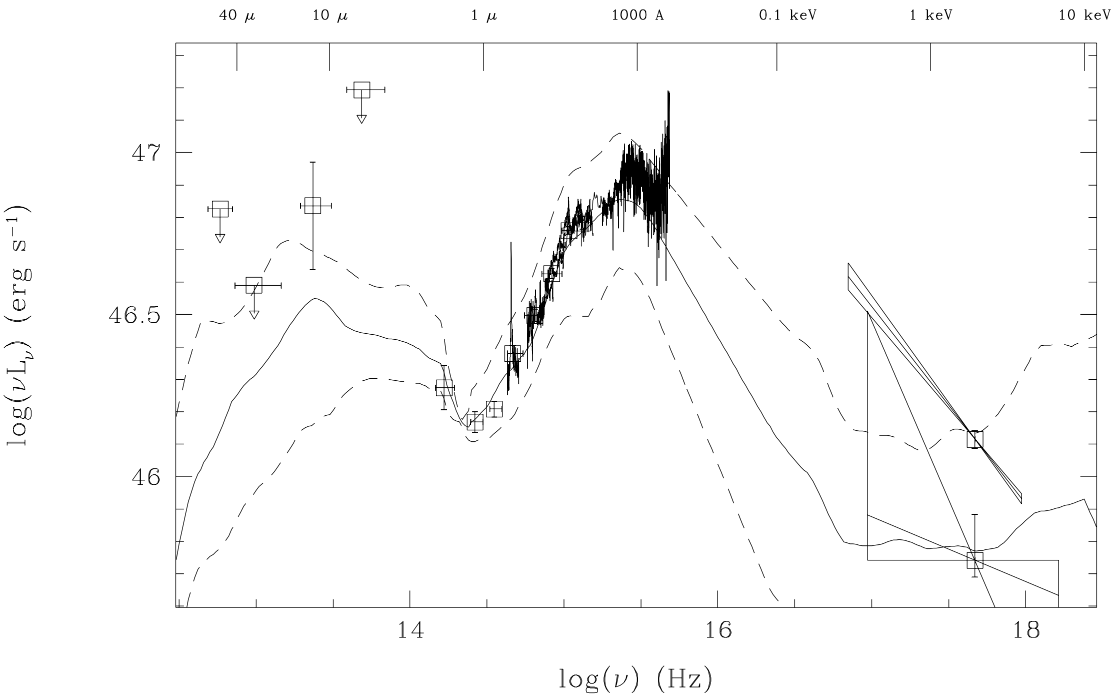

Fig. 7.— Rest frame spectral energy distribution for the quasar PG1407+265. Observations have been corrected for galactic foreground reddening with E(B-V)=0.03. The X-ray data points show power law fits to the Einstein and ROSAT data with 90 percent slope errors indicated. Solid and dashed lines indicate median quasar spectral energy distribution and 68 percentile deviations from Elvis et al (1994).

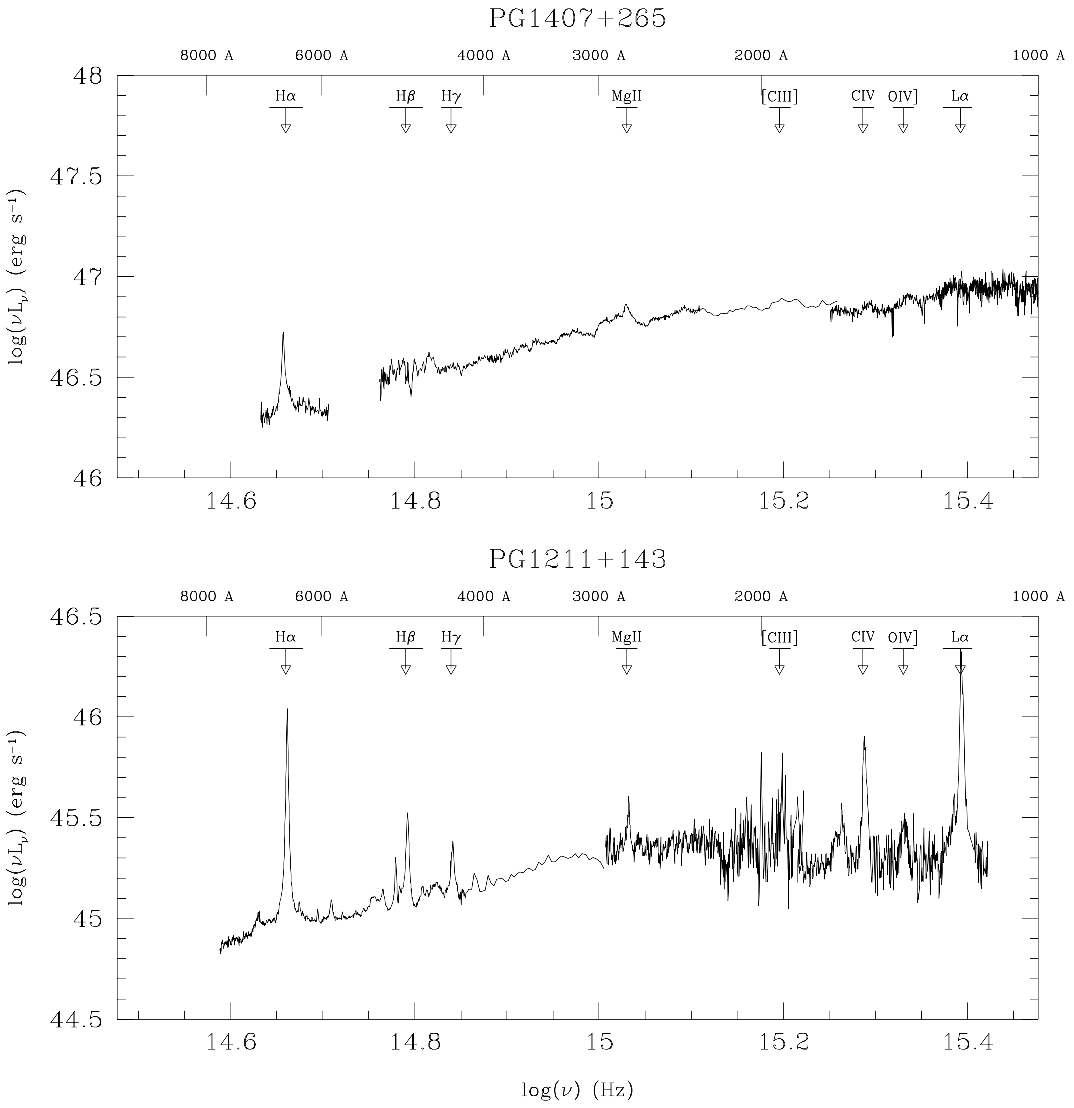

Fig. 8.— Optical and ultraviolet rest frame energy distribution for PG1407+265, compared with that of PG1211+143 (data from Elvis et al, 1994). The plots cover the same range in logarithmic flux, so lines of identical equivalent width will appear the same. Line identifications are indicated.